AD_____

Award Number: W81XWH-09-1-0406

TITLE: Development of a Hybrid Optical Biopsy Probe to Improve Prostate Cancer Diagnosis

PRINCIPAL INVESTIGATOR: Hanli Liu

CONTRACTING ORGANIZATION: University of Texas at Arlington
Arlington, TX 76019

REPORT DATE: June 2010

TYPE OF REPORT: Annual

PREPARED FOR: U.S. Army Medical Research and Materiel Command
Fort Detrick, Maryland 21702-5012

REPORT DOCUMENTATION PAGE

Form Approved
OMB No. 0704-0188

1. REPORT DATE	2. REPORT TYPE	3. DATES COVERED
1Jun 2010	Revised Annual	1 Jun 2009 - 31 May 2010

4. TITLE AND SUBTITLE

Development of a Hybrid Optical Biopsy Probe to Improve Prostate Cancer Diagnosis

5a. CONTRACT NUMBER

5b. GRANT NUMBER
W81XWH-09-1-0406

5c. PROGRAM ELEMENT NUMBER

6. AUTHOR(S)

Hanli Liu, Ph.D

Email: hanli@uta.edu

5d. PROJECT NUMBER

5e. TASK NUMBER

5f. WORK UNIT NUMBER

7. PERFORMING ORGANIZATION NAME(S) AND ADDRESS(ES)

The University of Texas at Arlington
Arlington, TX 76019

8. PERFORMING ORGANIZATION REPORT NUMBER

9. SPONSORING / MONITORING AGENCY NAME(S) AND ADDRESS(ES)

U.S. Army Medical Research and Materiel Command
Fort Detrick, Maryland 21702-5012

10. SPONSOR/MONITOR'S ACRONYM(S)

11. SPONSOR/MONITOR'S REPORT NUMBER(S)

12. DISTRIBUTION / AVAILABILITY STATEMENT

Approved for public release; distribution unlimited

13. SUPPLEMENTARY NOTES

14. ABSTRACT

Hypothesis: a multi-modal optical spectroscopic method and an integrated needle probe can be developed for guiding needle biopsy for prostate cancer diagnosis. Multi-modal optical measurements to be utilized for the study are (1) light scattering spectroscopy (LSS), (2) auto-fluorescence spectroscopy (AFS), and (2) auto-fluorescence life-time measurements (AFLT). Our specific aims are:

Aim 1: to develop a multi-modal, optical spectroscopic instrument, which allows the measurements of (1) LSS, (2) AFS, and (3) AFLT. The proposed system will be portable, can be used for in vivo measurements, and collect and present the data in real time. Aim 2: to integrate the optical fibers, which collect light scattering and auto-fluorescence from the prostate tissue, into a transrectal-ultrasound, needle-biopsy probe. In the development phase, the optical signatures of prostate cancer can be collected with the biopsy tissues and identified along every tract of needle biopsies. Aim 3: to collect optical signals of control and cancer tissues ex vivo along with the regular human needle biopsy, followed by classification algorithm development to discriminate cancer tissues. Aim 4: to perform in vivo measurement from human subjects to obtain the accuracy and sensitivity of the integrated probe in order to provide real-time, on-site, improved guidance for prostate cancer tissue biopsy.

15. SUBJECT TERMS

Technology Development, optical spectroscopy, transrectal probe, optical biopsy, auto-fluorescence spectroscopy, fluorescence life-time measurement.

16. SECURITY CLASSIFICATION OF: Unclassified			17. LIMITATION OF ABSTRACT	18. NUMBER OF PAGES	19a. NAME OF RESPONSIBLE PERSON
a. REPORT U	b. ABSTRACT U	c. THIS PAGE U		15	Hanli Liu 19b. TELEPHONE NUMBER (817) 272-2054

Standard Form 298 (Rev. 8-98)
Prescribed by ANSI Std. Z39.18

Table of Contents

2009-2010 Annual Progress Report

This report presents the specific aims and accomplishments of our prostate cancer research project during the year of funding sponsored by the US Department of the Army. It covers our activities from May 1, 2009 to August 31, 2010.

1. Introduction

It is known that effective treatments for prostate cancer are highly associated with accurate and early detection of prostate cancer. The current tools for detection of prostate cancer have serious shortcomings. So, the final diagnosis for prostate cancer relies on needle biopsy through transrectal-ultrasound guidance. Since ultrasound is not able to show any cancerous lesions, the current diagnostic needle biopsy for prostate cancer is rather "Blind": the biopsy samples were collected almost blindly without knowing whether or not the biopsy lesions are highly specious for cancer. The current diagnostic method in needle biopsy has three major deficiencies: (1) it may miss cancers that are present and have large high-grade lesion, (2) it can underestimate the severity of cancer that present, and (3) it may find only tiny low-grade cancers that likely do not cause problems. Because of these deficiencies, the current prostate cancer patients are either under or over treated: under treatments cause patients' lives; over treatments cause patients' unnecessary impotence or incontinence.

The hypothesis for this study is that a multi-modal optical spectroscopic method and an integrated needle probe can be developed for guiding needle biopsy for prostate cancer diagnosis. Multi-modal optical measurements to be utilized for the study are (1) light reflectance spectroscopy (LRS), (2) auto-fluorescence spectroscopy (AFS), and (2) auto-fluorescence life-time measurements (AFLM).

The project has four specific aims:

Aim 1: to develop a multi-modal, optical spectroscopic instrument, which allows the measurements of (1) LRS, (2) AFS, and (3) AFLM. The proposed system will be portable, can be used for in vivo measurements, and collect and present the data in real time.

Aim 2: to integrate the optical fibers, which collect light scattering and auto-fluorescence from the prostate tissue, into a transrectal-ultrasound, needle-biopsy probe. In the development phase, the optical signatures of prostate cancer can be collected with the biopsy tissues and identified along every tract of needle biopsies.

Aim 3: to collect optical signals of control and cancer tissues ex vivo along with the regular human needle biopsy, followed by classification algorithm development to discriminate cancer tissues.

Aim 4: to perform in vivo measurement from human subjects to obtain the accuracy and sensitivity of the integrated probe in order to provide real-time, on-site, improved guidance for prostate cancer tissue biopsy.

This report will summarize the work we performed from May 1, 2009 to August 2010 and the corresponding achievements obtained during this period of time, as given below.

2. Body of the Report

The PI and her research team have made significant efforts from 2009-2010 to accomplish the proposed aims, resulting in several published journal and conference papers. We will give a brief report in the following sub-sections.

2.1 Background

Prostate cancer is the most commonly found male cancer in the United States and is the second leading cause of death from cancer in men [1]. It was estimated that in 2009, the number of new prostate cancer cases reported would be 192,280, resulting in 27,360 deaths [2]. At present, digital rectal examination (DRE), prostate specific antigen (PSA) blood test and transrectal ultrasound (TRUS) guided biopsy are the clinically available techniques for prostate cancer screening and diagnosis. Among these, current gold standard for prostate cancer detection is TRUS guided needle biopsy, which involves resection of a core of prostate tissue with the guidance of an ultrasound probe. However, though ultrasound is able to provide anatomical images with high spatial resolution, it lacks the sensitivity in differentiating tumor from normal tissue, especially at early stages. This deficiency makes TRUS guided biopsy a rather "blind" procedure involving quasi-random sampling of the prostate tissue [3]. The implications of this drawback are false negatives, and oversampling of tissue due to non-specific targeting. A standard biopsy procedure involves resection of 10-12 cores, and it was believed that by increasing the number of core biopsies, the detection rate could be increased [4]. However, recent studies indicate that there is no significant improvement in detection rate by increasing number of biopsy cores (which is referred to as saturation biopsy [5,6]. Moreover, increasing the number of cores increases complications associated with the biopsy procedure [4]. It is therefore imperative to develop techniques that can identify the tumor in-vivo with high specificity and sensitivity and improve the accuracy of biopsy. It is even more crucial to develop a cancer-targeted diagnostic technique, which can identify the tumor on-site with high sensitivity and specificity.

Optical spectroscopic techniques can be a candidate for such needed tool to identify cancer from control. They may be implemented through needle probe geometry and will be extremely helpful in improving the diagnostic procedure. The first step in this study is to utilize an optical fiber which can be used to obtain *a priori* information by mapping the prostate tissue first, followed by subsequent biopsy of selected lesions. In this way, we can increase the accuracy of the biopsy procedure, substantially reduce the number of biopsy cores, and thus reduce the amount of tissue resected as well as minimize the associated complications. Specifically, two techniques have been implemented in such geometry in the past year: (1) light reflectance spectroscopy (LRS) and (2) auto-fluorescence lifetime measurement (AFLM).

LRS has been previously utilized for a variety of clinical applications by characterizing different tissue types using either empirical or analytical methods [7,8,9,10,11,12]. Recently, updated methods have been developed to quantify the absolute values of optical parameters from LRS with small probe geometries [9,13]. These analytical approaches make it more robust to be applied as a generalized means. On the other hand, various research groups have also implemented laser- induced, steady-state auto-fluorescence spectroscopy and time-resolved lifetime measurement for cancer detection [14]. Steady-state fluorescence measurements are easy to perform, however, they are intensity-dependent and thus sensitive to optical properties of tissue, ambient light, and excitation light intensity. We opted for temporally-resolved fluorescence lifetime measurements as they are independent of absolute intensity of excitation light and fluorophore concentration.

2.2 Report for Aim 1

Aim 1: develop a multi-modal, optical spectroscopic instrument, which allows the measurements of (1) LRS, (2) AFS, and (3) AFLM. The proposed system will be portable, can be used for in vivo measurements, and collect and present the data in real time.

For this aim, we have implemented and evaluated both LRS and AFLM systems independently, to differentiate between cancer and non-cancerous tissue using laboratory tissue phantoms. LRS is used to calculate the absolute concentrations of oxy-hemoglobin, deoxy-hemoglobin and scattering properties of the tissue. AFLM uses a custom built device to measure auto-fluorescence lifetime of the tissue. We have tested the efficacy of using these multiple parameters as classifiers to identify prostate cancer. The results are presented in this report and provide us with the footprints for future ex-vivo and in-vivo human prostate cancer measurements.

2.2.1 Laboratory tissue phantoms and preparation

Phantom measurements were carried out to test our newly implemented LRS and AFLM system for this part of study. Figure 1 shows the diagram of the combined system with a tissue phantom. To create a homogenous phantom, a blood-intralipid solution was made by diluting a stock intralipid solution (concentration=20%, Baxter Healthcare Corporation, Deerfield, IL) with phosphate buffered saline (PBS) and de-fibrinated horse blood (Hemostat Laboratories, Dixon, CA). We varied the concentrations of intralipid and blood, to obtain various combinations of scattering and absorption properties. To simulate hemodynamic changes in the phantom, 4 mg of yeast was added into a 3-liter liquid phantom to deoxygenate the blood-containing phantom. When the phantom was fully deoxygenated, 100% oxygen was slowly bubbled into the solution to re-oxygenate it. Overall, we could simulate changes in light scattering by alternating intralipid concentrations and mimic changes in light absorption by modifying either the blood volume or oxygenation state. In the tumor-simulating experiments, we increased the light absorption by 2-3 times higher than that from the baseline (healthy-tissue) phantoms to detect the differences in both LRS and AFL.

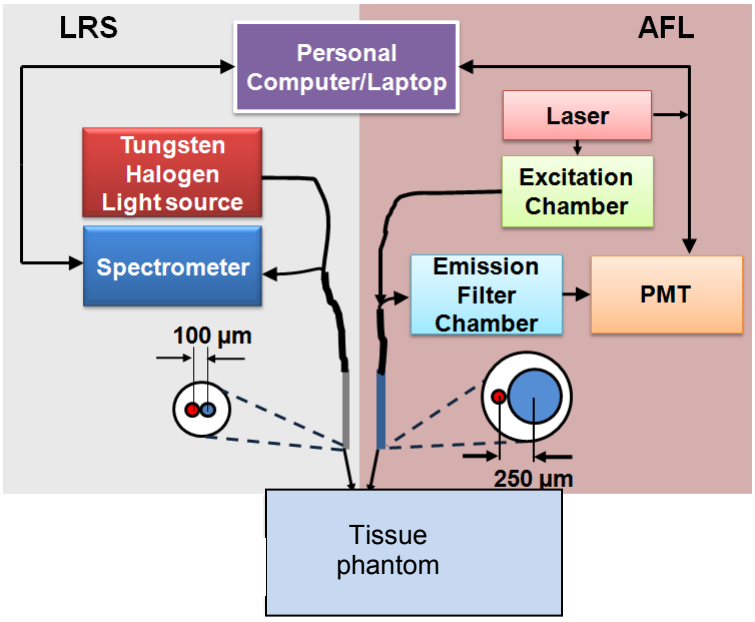

Fig. 1 A block diagram illustrating experimental set-up for LRS system (left) and AFLM system (right). Measurements were made sequentially, by placing the fiber tips on the tissue phantom surface. A closer view of bi-furcated fiber tips are shown for each fiber (red = source; blue = detector).

2.2.2 Auto-florescence lifetime measurement

AFLM Instrumentation

For auto-florescence lifetime measurements, a custom-made, single-channel, Time Correlated Single Photon Counting (TCSPC) system (ISS Inc., Champaign, IL) was employed. Fig. 1 (right) shows an overall experimental setup for the time domain AFLM. The system consisted of a 5-slot filter wheel for excitation wavelength selection (which was driven by a 12-V-powered stepper motor), an emission filter, a continuously variable neutral density (ND) filter for excitation light intensity control, and a highly sensitive cooled PMT (Becker & Hickl GmbH) with wavelength sensitivity between 125 – 850 nm. The PMT gain was controlled via PC-based card (DCC-100). A picoseconds (ps) broadband (400 – 1800 nm) pulsed laser (SC - 450, Fianium Inc., Eugene, Oregon) was used as an excitation source at the repetition rate of 20 MHz. Precise synchronization between the incoming laser pulse and photon event was achieved through a PC-based single photon counting card (SPC-130). As shown in Fig. 1, the laser was coupled to the source fiber of the bi-furcated optical probe (core diameter 100 μm); resulting fluorescence emission was collected through the detector fiber (400 μm core diameter).

AFLM Data Analysis

In this part of study, we were mainly targeting auto-fluorescence from Flavins, Lipo-pigments and Porphyrins as a contrast parameter to differentiate cancer from healthy tissue. In order to achieve maximum possible auto-fluorescence from all three endogenous compounds, an excitation wavelength of 447 nm was chosen [15]. While keeping the excitation wavelength constant, the emission wavelengths were changed between 532 nm, 562 nm, 632 nm and 684 nm. Data collection was done through Vinci software provided by ISS. The optical probe was placed at ~1 mm away from the surface of the tissue phantom; the fluorescence data were collected at 5 random positions from the phantom for each emission wavelength. The detected fluorescence decay was imported into Matlab (The Mathworks Inc., Natick, MA) and normalized with respect to peak intensity.

In order to quantitatively differentiate auto-fluorescence decay of cancer and control, each curve can be fitted (least square non-linear fitting algorithm) using a two-component exponential model, as given by:

$$Intensity(I) = \sum_i \alpha_i e^{-\frac{t}{\tau_i}}, \qquad (1)$$

where, τ_i (i=1, 2) indicates lifetime of each component and α_i (i=1, 2) is intensity contribution of each component to the overall fluorescence decay. The confidence interval for each of these four fitted parameters was computed using the "confint" function in Matlab. In order to make the comparison between normal and cancerous tissue, the mean lifetime, $<\tau>$, was calculated using equation 2:

$$<\tau> = \frac{\sum_i \alpha_i \times \tau_i^2}{\sum_i \alpha_i \times \tau_i} \qquad (2)$$

2.2.3 Light Reflectance spectroscopy

LRS Instrumentation

The LRS system consisted of a tungsten-halogen light source (HL2000HP, Ocean Optics, Dunedin, FL, USA), a CCD array spectrometer (USB 2000+, Ocean Optics, Dunedin, FL USA), and a laptop computer. The spectrometer provided a spectrum ranging from 460 nm-1150 nm. A custom-made, bi-furcated, fiber optic probe (Fiberguide Industries, Stirling, NJ, USA) was designed and implemented with source and detector diameters of 100 μm, center-to-center source and detector separation of ~100 μm, and an outer probe diameter of 800 μm. The probe was fixed on a stereotactic frame in order to control the probe tip position and minimize the pressure on the tissue surface. Multiple data points were obtained by placing the probe at different spatial locations on the healthy-tissue phantoms and then the tumor-simulating tissue phantoms. On an average, 5 data points were obtained for each tissue phantom type.

LRS Data Acquisition and Analysis

Each acquired spectrum was divided by a reflectance spectrum obtained from a diffuse reflectance standard (WS-1, Ocean Optics, Dunedin, FL, USA) to eliminate the spectral effect from the light source, optical fibers and CCD array detector from the reflectance spectrum taken from the tissue sample. Figure 2 shows a schematic diagram for the setup. For system calibration, we utilized a gold-standard, dual-channel, tissue oximeter (ISS, Inc., IL, USA), as also shown in Fig. 2. The ISS oximeter could provide absolute values of optical properties for the measured sample under light interrogation, thus providing calibration parameters to LRS.

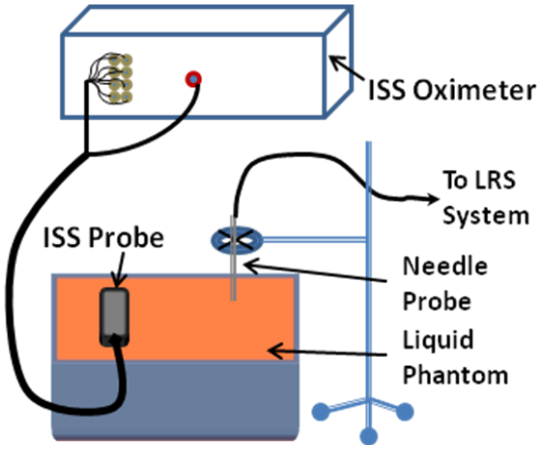

Figure 2

Then, the spectral range from 500 nm - 850 nm was selected and a reflectance model [9] as shown in equation (3) was utilized to obtain absolute values of the concentrations of oxy-hemoglobin ([HbO]), deoxy-hemoglobin ([HbR]) and total hemoglobin ([HbT] = [HbR] + [HbO]), along with the reduced scattering coefficient (μ_s').

$$R_p(\lambda) = \frac{\mu_s'(\lambda)}{k_1 + k_2 \cdot \mu_a(\lambda)}, \qquad (3)$$

where R_p is the measured reflectance, μ_s' is the reduced scattering coefficient, μ_a is the absorption coefficient depending on the concentration of hemoglobin derivatives and k_1 and k_2 are calibration constants that depend on the probe geometry and hardware set-up. A detailed description of methods to obtain the above parameters has been previously published [7]. Briefly, at first, k_1 and k_2 were calculated for the specific fiber optic probe using tissue phantom calibration. Then, an optimization routine [16] (ant colony optimization) was used to obtain the parameters of μ_s' at 750 nm, [HbO] and [HbR], by achieving the best fit for the measured reflectance. The data processing was implemented and executed in Matlab. Specifically, we provide details on data analysis/process procedures as follows.

(1) Quantification of hemoglobin concentrations:

It is well known that $\mu_a(\lambda)$ is a function of concentrations of deoxygenated hemoglobin, [Hb], oxygenated hemoglobin, [HbO], and water, H_2O. The spectral dependence of μ_a on [HbO], [Hb], and H_2O for blood-perfused tissues can be written as

$$\mu_a(\lambda) = [HbO]\,\varepsilon_{HbO}(\lambda) + [Hb]\,\varepsilon_{Hb}(\lambda) + [\%H_2O]\varepsilon_{H_2O}(\lambda), \quad (4)$$

where 'λ' is the wavelength in nm, $\varepsilon_{HbO}(\lambda)$, $\varepsilon_{Hb}(\lambda)$ and $\varepsilon_{H2O}(\lambda)$ are the wavelength dependent extinction coefficients of [HbO], [Hb], and water, respectively. [$\%H_2O$] represents the percentage of water in the medium. Other chromophores, such as fat and melanin, may be added to this equation, depending on the wavelength range of interest and tissue type under investigation. The spectral dependence of μ_s' can be approximated as given by Mie theory [17]:

$$g = 1.1 - (0.58\times10^{-3})\lambda, \quad (5)$$

$$\mu_s' = \mu_s(1-g), \quad (6)$$

$$\mu_s = a\lambda^{-b}, \quad (7)$$

where μ_s is the effective scattering coefficient, μ_s' is the reduced scattering coefficient, and g is the anisotropy factor. In eq. (7), parameters of a and b are constants and depend on scatterer sizes and types. For 10% intralipid solution, the calculated values are a = 2.54x10^9 cm^{-1} and b = 2.4 [17].

(2) Calculation and calibration of k_1 and k_2

In this study, we determined the values of k_1 and k_2 using the least-squares regression approach. By rearranging (3), we obtain

$$\frac{\mu_s'(\lambda)}{R_p(\lambda)} = k_1 + k_2\mu_a(\lambda)\,. \quad (8)$$

This equation shows that k_1 and k_2 can be determined by obtaining a linear regression line that best fits $\mu_s'(\lambda)/R_p(\lambda)$ versus $\mu_a(\lambda)$. In principle, we can obtain the measured spectra of $R_p(\lambda)$ from the LRS system within 500-850 nm and also achieve quantification of μ_a and μ_s' at 750 nm and 830 nm from ISS oximeter if the measurements by both LRS and ISS oximeter are taken simultaneously. Besides μ_a values, ISS oximeter is also able to provide derived values of [Hb], [HbO], and μ_s' at two wavelengths (OxiplexTS). Then, wavelength-dependent absorption spectra, $\mu_a(\lambda)$, can be quantified using eq. (4) if the measured [Hb] and [HbO] as well as the hemoglobin extinction coefficients are available. Moreover, given two μ_s' values at two measured wavelengths (750 nm and 830 nm), it is reasonable to interpolate and extrapolate $\mu_s'(\lambda)$ over the desired wavelength range using eqs. (5)-(7) based on Mie theory.

During the system calibration in the study, we followed the exact principle or procedures given above to acquire $R_p(\lambda)$, $\mu_a(\lambda)$, and $\mu_s'(\lambda)$ from a set of blood-containing tissue phantoms. A corresponding set of k_1 and k_2 at various total hemoglobin concentrations and reduced scattering coefficients were obtained, averaged, and calculated for their means and standard deviations. If the relative errors for both k_1 and k_2 were less than 10% (i.e., standard deviations divided by their means) , then the corresponding set of k_1 and k_2 were finalized as the system calibration parameters for the specific LRS system (i.e., the light source, fiber probe, and spectrometer) chosen for this study.

As an example, Fig. 3(a) shows a set of measured $R_p(\lambda)$, $\mu_a(\lambda)$, and $\mu_s'(\lambda)$ (blue symbols) and the linear regression line (red thick line) for our LRS probe with k_1 being the y-intercept and k_2 being the slope. While the inverse calculations for an unknown sample will be described in

the next sub-section, an illustration of the measured and fitted reflectance is shown in Fig. 3(b). The accuracy of parameters k_1 and k_2 critically affects the 'goodness of fit' in the inverse calculations, and thus influences the accuracy of measured optical properties of tissues under interrogation. It is noteworthy to point out that k_1 and k_2 depend highly on the white sample measurement for eliminating instrumentation effects on the measured spectrum of the sample under examination. Incorrect measurement of the white sample will lead to serious errors for the fitted parameters, i.e., [Hb], [HbO], *a* and *b* in eq. (7).

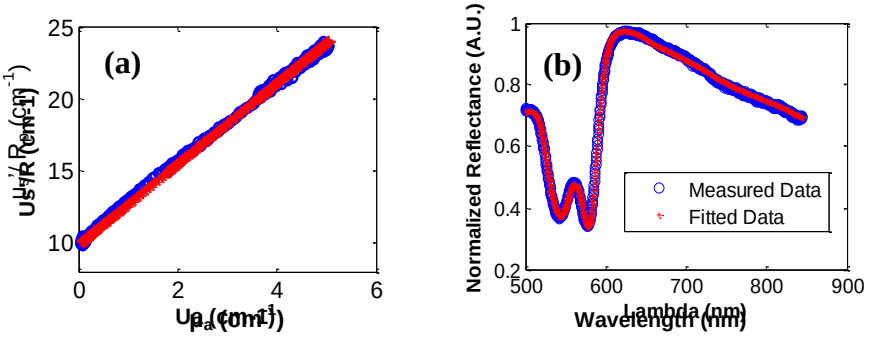

Figure 3

White sample measurement can vary with the following parameters: distance between the fiber tip and sample surface, integration time, light source intensity. Measuring different types of tissue requires a different integration time for the detector. Fig 4 shows the measurement geometry from the white sample. Since the reflectance curve needs to be divided by the reference curve from the white sample, care should be taken to standardize the procedure. This can be done either by fixing the distance and collecting white sample at various integration times to create a look-up table, or by scaling the white sample reflectance curve based on one single measurement. The latter method is based on our observation that the relationship between reflectance spectra and integration times is approximately linear.

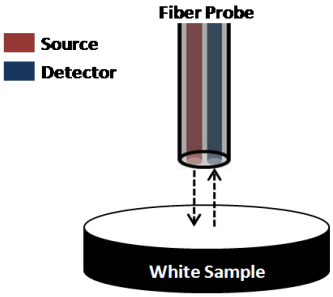

Figure 4

(3) *Inverse calculation*

The inverse calculation of eq. (3) deals with determination of tissue chromophore concentrations and effective scattering coefficients from the measurements of LRS taken on the tissue surface. The mathematical problem of inversion can be practically solved by an approach of function minimization using an optimization algorithm. The algorithm searches for an optimal set of values, as represented by $\boldsymbol{x}$=([Hb], [HbO], *a*, *b*), from the given multi-parameter space that best match the measured $R_p(\lambda)$ using the least- squares analysis. It can be mathematically expressed as follows:

$$f(x) = \sum_{i=1}^{M} \left[R_p(\lambda_i)^{(measured)} - R_p(\lambda_i)^{(predicted)} \right]^2, \qquad (9)$$

where $f(\boldsymbol{x})$ represents an objective function and needs to be minimized by finding an optimal set of the parameters, $\boldsymbol{x}_{opt}$, M is the number of wavelengths, $R_p(\lambda_i)^{(measured)}$ and $R_p(\lambda_i)^{(predicted)}$ are the reflectance values (at wavelength λ_i) measured by the optical probe and predicted by eqs. (3) to (7), respectively, with the parameter set, $\boldsymbol{x}$, to be optimized. Evolutionary algorithms are widely utilized in the field of optimization. The algorithms work on a population of values rather an initial guess, making the solution independent of an initial guess. Their inherent characteristics make them suitable to search for a global minimum, rather than being stuck in local minima. The ant colony optimization (ACO) algorithm, introduced by M. Dorigo [18], is a probabilistic evolutionary

technique for solving computational problems. This basic technique was modified in this study to suit function minimization [16].

Equation (3) is very non-linear and spanned from 500 nm to 850 nm. In order to obtain optimal fit between the measured and calculated reflectance curve, we had to incorporate multiple sequences, within each of which the objective function for minimization, eq. (9), was selected somewhat differently. First, the entire spectrum (500 nm – 850 nm) was utilized for fitting and the fitted values of [Hb], [HbO], *a* and *b* in eq. (7) were obtained. Next, the $\mu_s(\lambda)$ values (or *a* and *b)* were fixed with 15% bounds used in sequence one. A smaller spectral region of 520-590 nm that has a strong hemoglobin absorption band was selected for re-fitting to improve 'goodness of fitting' for [Hb] and [HbO]. Finally, after refining the fitted parameters of [Hb] and [HbO], they were fixed within 20% bounds used in sequence two. The entire spectrum (500-850 nm) was re-fitted, leading to the finally optimized values of [Hb], [HbO], *a* and *b*. Overall, three fitting sequences with changing parameter bounds and spectral regions were utilized in order to obtain an optimal fit for scattering and absorption parameters. An example to show comparison between the measured and fitted reflectance is already given in Fig. 3(b).

2.2.4 Results:

Algorithm validation for absolute quantification by LRS

In order to validate the algorithm for absolute quantification, we created tissue phantoms and performed the measurements with both our single-channel LRS system and a tissue oximeter (ISS Oximeter), which was used as a gold standard device for comparison. Figure 5(a) shows comparisons between the values obtained from ISS tissue oximeter and those quantified with our method when a change in oxygen saturation(O_2 Sat) was achieved by adding yeast to the liquid phantom. The measurements were made at 12 different time points in the O_2 Sat range of ~20%-80% during the oxygenation and deoxygenation process. It is clear from Fig. 5(a) that oxygen saturation(O_2 Sat) values measured by both modalities are very consistant in the O_2 Sat range of 20%-80%. The absolute errors were also calculated at each data point (n=12) and are plotted in Fig. 5(b): average absolute errors for O_2 Sat, [Hb] and [HbO], along with standard error of mean (SEM) were 3.0±0.7 %, 0.9±0.2 μM, and 0.9±0.2 μM, respectively. Similar experiments were repeated several times, and the results were very similar to those seen in Figs. 5(a) and 5(b).

The reliability of the algorithm was also evaluated by comparing the changes in total hemoglobin concentration, [HbT], and μ_s' for each set of the above measurement. Since yeast did not induce much change in either [HbT] or μ_s', these two parameters should ideally remain constant when the oxygenation state was altered. Figure 5(c) shows the measured values of [HbT] and μ_s' (at 750 nm and 830 nm) with changing O_2 Sat. As expected, those values are found to be constant across the saturation range of 20-80% with small SEMs as [HbT] = 28.0 ±0.4 μM, μ_s' (750 nm) = 10.46±0.05 cm^{-1}, and μ_s' (830 nm) = 9.34±0.04 cm^{-1}. Another set of experiments were conducted to test the consistancy of μ_s' when Intralipid volume was varied from 75 ml to 170 ml within the given liquid phantom volume. Figure 5(d) shows a comparison of values obtained by the ISS oximeter and LRS system at 830 nm. The mean difference (with standard deviation) between the scattering values obtained by two methods was calculated to be 0.02±0.13 cm^{-1}, demonstrating almost perfect match between the two methods.

After comprehensive algorithm validation for LRS, we were able to quantify optical properties and hemodynamic parameters, namely μ_a, μ_s', [HbO], and [HbT], of interrogated tissues by the optical probe. The LRS system was ready for studies using *ex vivo* human prostate specimens.

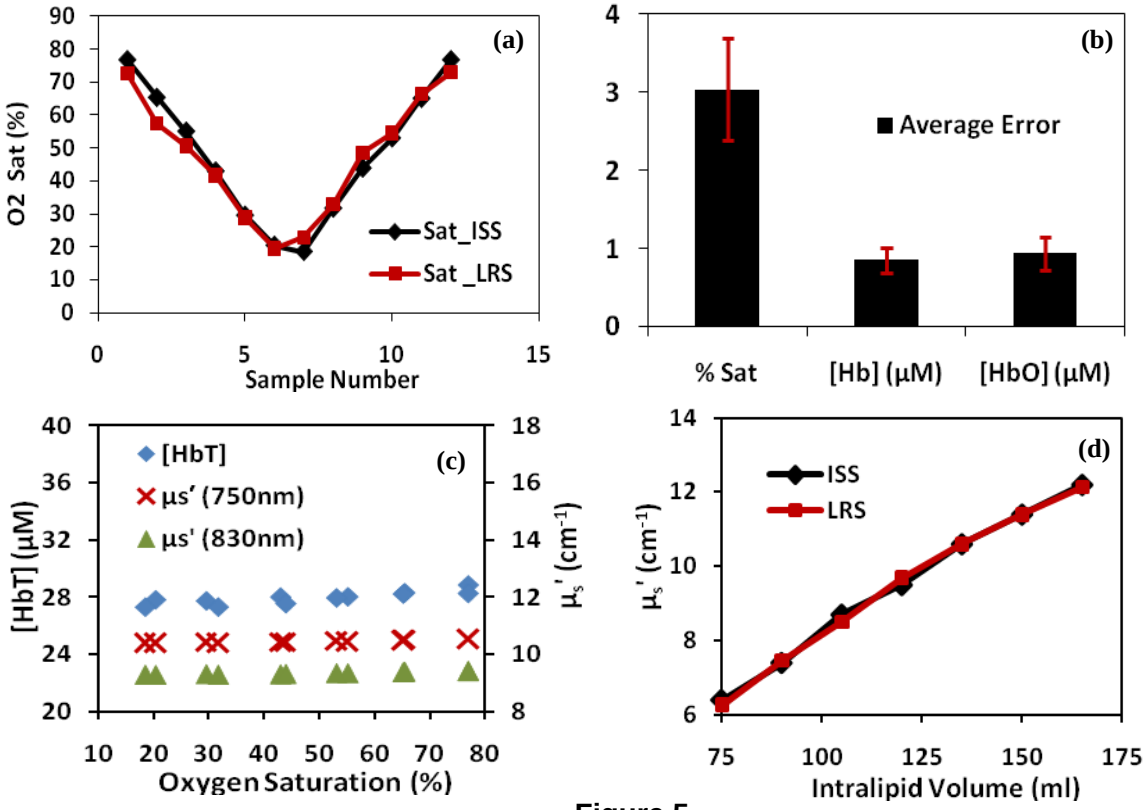

Figure 5

For AFLM results, we did not obtain too much meaningful results, possibly because our tissue phantoms are highly hemoglobin-based and are not a good light fluorescence tissue model. As mentioned earlier, the auto-fluorescence contrast comes mainly from Flavins, Lipo-pigments and Porphyrins. Our current tissue phantoms did not include much of those components. The system would be better tested and validated when we are ready for *ex vivo* human prostate specimen measurements.

2.3 Report for Aim 2

Aim 2: to integrate the optical fibers, which collect light scattering and auto-fluorescence from the prostate tissue, into a transrectal-ultrasound, needle-biopsy probe. In the development phase, the optical signatures of prostate cancer can be collected with the biopsy tissues and identified along every tract of needle biopsies.

For Aim 2, we have completed and implemented the 1st version of an integrated optical-fiber assembly that is under testing to collect both LRS and AFLM. The detailed design is given below:

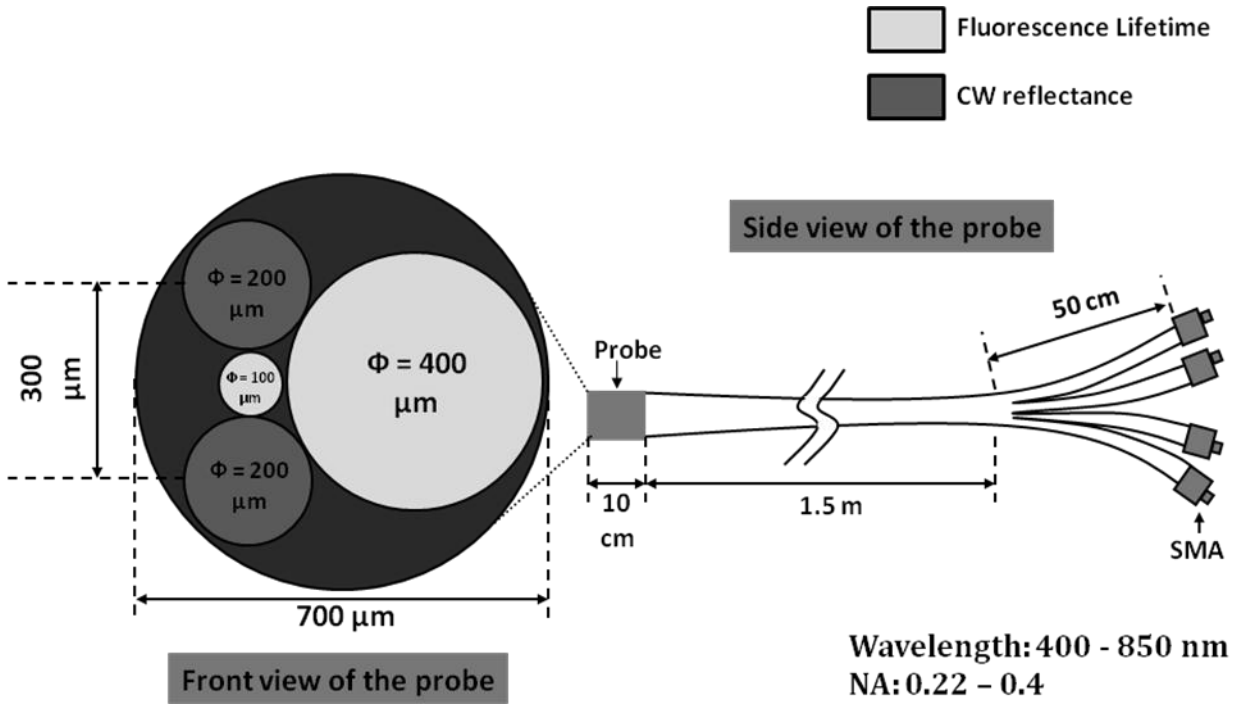

3. Key Research Accomplishments and Reportable Outcomes

(1) Successfully developed a multi-modal, optical spectroscopic instrument, which allows the measurements of (1) LRS, (2) AFS, and (3) AFLM. The individual systems have been tested using laboratory tissue phantoms.

(2) Two related research works are published:

(a) Anindita Mukerjee, Rafal Luchowski, Amalendu P. Ranjan, Sangram Raut, Jamboor K. Vishwanatha, Zygmunt Gryczynski, and Ignacy Gryczynski, "Enhanced Fluorescence of Curcumin on Plasmonic Platforms," *Current Pharmaceutical Biotechnology*, ***11***, 223-228 (2010).

(b) Anindita Mukerjee, Thomas J. Sørensen, Amalendu P. Ranjan, Sangram Raut, Ignacy Gryczynski, Jamboor K. Vishwanatha, and Zygmunt Gryczynski,"Spectroscopic Properties of Curcumin: Orientation of Transition Moments," *J. Phys. Chem. B*, ***114***, 12679–12684 (2010).

4. Conclusions and plan for next year

In summary, for the period from May 2009 to August 2010, we have implemented two separate units for AFLM and LRS and demonstrated that both AFLM and LRS are feasible methods to collect good optical signals from tumor-simulating tissue phantoms. However, the AFLM results from tissue phantoms may not truly reflect the actual signals collected from the human prostates. Further measurements from human prostate specimens will be explored in the following year. On the other hand, the LRS results are much reliable and reflect the differences between healthy and tumor tissues more realistically than those in AFLM. The sensitivity and specificity of this technique is also reasonably high; the technique may allow deeper tissue measurements, as compared to AFLM, depending on [HbR] levels in the tumor.

In the coming year, we will carry on the development for Aim 2 and Aim 3: (1) to integrate the optical fibers, which collect light scattering and auto-fluorescence from the prostate tissue, into a

combined, needle-biopsy probe; (2) to collect optical signals of control and cancer tissues ex vivo along with the regular human needle biopsy, followed by classification algorithm development to discriminate cancer tissues.

5. References

1. A. Jemal, R. Siegel, E. Ward, Y. Hao, J. Xu and M. J. Thun, "Cancer statistics, 2009," CA Cancer J Clin 59(4), 225-249 (2009).
2. A. C. Society, "Cancer Facts and Figures 2009," Atlanta: American Cancer Society (2009).
3. N. B. Delongchamps and G. P. Haas, "Saturation biopsies for prostate cancer: current uses and future prospects," Nat Rev Urol 6(12), 645-652 (2009).
4. U. Patel, "TRUS and prostate biopsy: current status," Prostate Cancer Prostatic Dis 7(3), 208-210 (2004).
5. A. Descazeaud, M. Rubin, S. Chemama, S. Larre, L. Salomon, Y. Allory, D. Vordos, A. Hoznek, R. Yiou, D. Chopin, C. Abbou and A. de la Taille, "Saturation biopsy protocol enhances prediction of pT3 and surgical margin status on prostatectomy specimen," World J Urol 24(6), 676-680 (2006).
6. J. S. Jones, A. Patel, L. Schoenfield, J. C. Rabets, C. D. Zippe and C. Magi-Galluzzi, "Saturation technique does not improve cancer detection as an initial prostate biopsy strategy," J Urol 175(2), 485-488 (2006).
7. V. Sharma, D. Kashyap, A. Mathker, S. Narvenkar, K. Bensalah, W. Kabbani, A. Tuncel, J. A. Cadeddu and H. Liu, "Optical reflectance spectroscopy for detection of human prostate cancer," Conf Proc IEEE Eng Med Biol Soc 2009, 118-121 (2009).
8. H. Liu, H. Radhakrishnan, A. K. Senapati, C. E. Hagains, D. Peswani, A. Mathker and Y. B. Peng, "Near infrared and visible spectroscopic measurements to detect changes in light scattering and hemoglobin oxygen saturation from rat spinal cord during peripheral stimulation," Neuroimage 40(1), 217-227 (2008).
9. G. Zonios and A. Dimou, "Modeling diffuse reflectance from semi-infinite turbid media: application to the study of skin optical properties," Opt Express 14(19), 8661-8674 (2006).
10. C. A. Giller, H. Liu, D. C. German, D. Kashyap and R. B. Dewey, "A stereotactic near-infrared probe for localization during functional neurosurgical procedures: further experience," J Neurosurg 110(2), 263-273 (2009).
11. M. Johns, C. Giller, D. German and H. Liu, "Determination of reduced scattering coefficient of biological tissue from a needle-like probe," Opt Express 13(13), 4828-4842 (2005).
12. K. Bensalah, D. Peswani, A. Tuncel, J. D. Raman, I. Zeltser, H. Liu and J. Cadeddu, "Optical reflectance spectroscopy to differentiate benign from malignant renal tumors at surgery," Urology 73(1), 178-181 (2009).
13. S. C. Kanick, C. van der Leest, J. G. Aerts, H. C. Hoogsteden, S. Kascakova, H. J. Sterenborg and A. Amelink, "Integration of single-fiber reflectance spectroscopy into ultrasound-guided endoscopic lung cancer staging of mediastinal lymph nodes," J Biomed Opt 15(1), 017004.
14. P. K. M. Katika, L. Pilon, K. Dipple, S. Levin, J. Blackwell and H. Berberoglu, “In vivo time-resolved autofluorescence measurements on human skin,” Proc. SPIE 6078, 60780L (2006).
15. G.A. Wagnières, W.M. Star and B.C. Wilson, "In vivo fluorescence spectroscopy and imaging for oncological applications," Photochem Photobiol 68(5), 603-632 (1998).
16. D. Kashyap, "Development of a Broadband Multi-Channel NIRS System for Quantifying Absolute Concentrations of Hemoglobin Derivatives and reduced scattering Coefficients," Thesis dissertation (2007).

17. van Staveren, H.J., Moes, C.J.M., van Marie, J., Prahl, S.A., van Gemert, M.J.C., 1991. Light scattering in Intralipid-10% in the wavelength range of 400–1100 nm. Applied Optics 30, 4507-4514.
18. Dorigo, M., Maniezzo, V., Colorni, A., 1996. Ant system: optimization by a colony of cooperating agents. IEEE Trans Syst Man Cybern B Cybern 26, 29-41.